ANALYSIS OF SHADED POLE INDUCTION MOTORS CONSIDERING ASYMMETRICAL FLUX DISTRIBUTION AND SATURATION EFFECTS

J. Faiz, M. R. Feyzi and A. Abbasi

Department of Electrical Engineering
Faculty of Engineering
University of Tabriz
Tabriz, Iran

Abstract Several methods are available for performance prediction of single phase shaded pole induction motors. A simple model, in conjunction with a more complicated and accurate model, which considers the asymmetrical windings and core loss, is used to compare the prediction methods against experimental results. Saturation is incorporated in the model. Fundamental and harmonic flux density wave distributions under the pole are determined by employing the accurate mathematical model of the motor and the influence of the shading angle upon this distribution is shown. The effect of airgap length upon the torque speed characteristic of the motor is also investigated.

Key Words Induction Motor, Shaded Pole, Single Phase Motor, Saturation Effect, Asymmetrical Windings

چکیده روشهای متعددی برای پیش بینی عملکرد موتورهای القایی تکفاز با قطب چاکدار وجود دارد. یک مدل ساده همراه با یک مدل پیچیده تر و دقیق تر که در آن سیم پیچی های نامتقارن و تلف هسته مدنظر قرار گرفته، بکار رفته و این روش های تخمینی با نتایج تجربی مقایسه شده اند. اشباع در مدل منظور گردیده است. توزیع موج چگالی فلوی اصلی و هارمونیک ها در زیر قطب به کمک مدل ریاضی دقیق موتور تعیین می شوند و تأثیر زاویه سایه بان برروی این توزیع نشان داده می شود. تأثیر طول فاصله هوایی برروی مشخصه های گشتاور / سرعت موتور نیز مورد بررسی قرار می گیرد.

INTRODUCTION

Shaded pole induction motors are widely used for fractional horsepower applications. The simple construction, high reliability and low cost are the major reasons for their wide applicability. The windings of the motor are asymmetrical resulting in a non-sinusoidal airgap field distribution and, therefore, space harmonics. Trickey [1,2] has presented one of the earliest analyses of the motor. Chang [3] and Ooka [4] have derived equivalent circuits. The effects of various parameters, such as shading-coil resistance on the steady state peformance have been investigated [5, 6]. A method for torque prediction [7], as well as a method for calculating the effects caused by space harmonic MMFs on the torque-speed characteristics has been published.

In the present work, the early theoretical analysis by Trickey [1,2] and a recent analysis by Singh [8] are employed for performance prediction of the motor. The theoretical results are then compared with experimental results. To perform this, two computer programs have been developed and experimental data have been obtained by testing a typical shaded pole induction motor. A mathematical model has been used to predict the magnetic flux density distributions under the salient pole of the motor for different conditions. The influence of the shading angle upon the field distribution is shown. The effects of saturation upon the motor performance have been

studied. Comparison between the predicted and measured performance leads to a realistic value of saturation factor. Performance variations with airgap length is studied and discussed.

EQUIVALENT CIRCUITS OF THE MOTOR

Two equivalent circuit models, one based on the Trickey method [1, 2] (the "first method" henceforth) and the other based on the Singh method [8], (the "second method" henceforth) are used. In the first method, an equivalent circuit for the fundamental sinusoidal flux is employed and core loss is ignored. In the second model, backward and forward components of the pole flux are considered in the equivalent circuit (odd components)

The fields of auxiliary and main windings are decomposed into forward and backward fields resulting in four rotating fields in the airgap. An improved equivalent circuit, taking into account the space harmonic flux density, has been shown in Figure 1 [8]. Forward (x = f) and backward (x = b) torques are calculated as follows:

$$T_x = \sum_{n=1}^{n} \mathrm{Re}\,[n\,|I_{xn}|^2 Z_{xn}] \qquad (1)$$

EXPERIMENTAL TEST SETUP

The experimental arrangement for the proposed shaded pole induction motor is depicted in Figure 2. The torque of motor is converted into voltage by a strain gauge. The converted torque and speed into frequencies are fed to the amplifier. The outputs of the amplifier are the inputs of the PC through an hardware (interface). The torque slip characteristic can be plotted using a plotter.

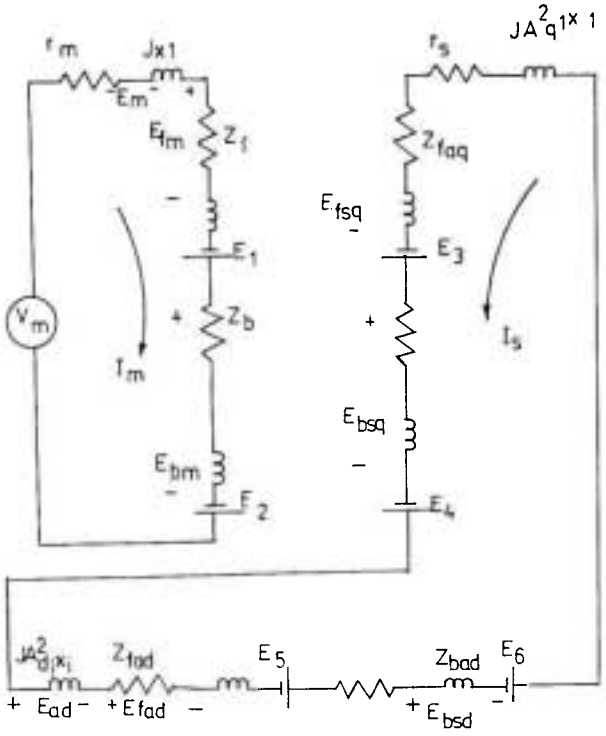

$K_{wmn} = \sin(n\theta_m/2)$, $K_{wsn} = \sin(n\theta_m/2)$

$A_{dn} = A_n \mathrm{Cos}(n\theta)$, $A_{qn} = A_n \sin(n\theta)$, $A_n = K_{wsn} / (N_m K_{wmn})$

$Z_{fsq} = \Sigma A_{qn}{}^2 Z_{fn}$, $Z_{bsq} = \Sigma A_{qn}{}^2 Z_{bn}$

$Z_{fsd} = \Sigma A_{dn}{}^2 Z_{fn}$, $Z_{bsd} = \Sigma A_{dn}{}^2 Z_{bn}$

$Z_f = \Sigma Z_{fn}$, $Z_b = \Sigma Z_{bn}$

$E_{fm} = \Sigma I_m Z_{fn} + \Sigma I_s A_{dn} Z_{fn}$

$E_{bm} = \Sigma I_m Z_{bn} + \Sigma I_s A_{dn} Z_{bn}$

$E_{fsd} = A_{dn} E_{fm}$, $E_{bsd} = A_{dn} E_{bm}$

$E_{fsq} = \Sigma I_s A_{qn}{}^2 Z_{fn}$, $E_{bsq} = \Sigma I_s A_{qn}{}^2 Z_{bn}$

$r_m = r_1 r_{fm} / (r_1 + r_{fm})$

$v_m = r_1 V_{rfm} / (r_1 + r_{fm})$

$r_s = r_a r_{fs} / (r_a + r_{fs})$

Figure 1. An accurate equivalent circuit of a shaded pole induction motor.

COMPARISON OF PERFORMANCE PREDICTION METHODS

The predicted torque using the two methods over the whole range of slip is compared with the experimentally obtained torque. The predicted results, in the range of T_{st} to T_{po}, are in good agreement with the

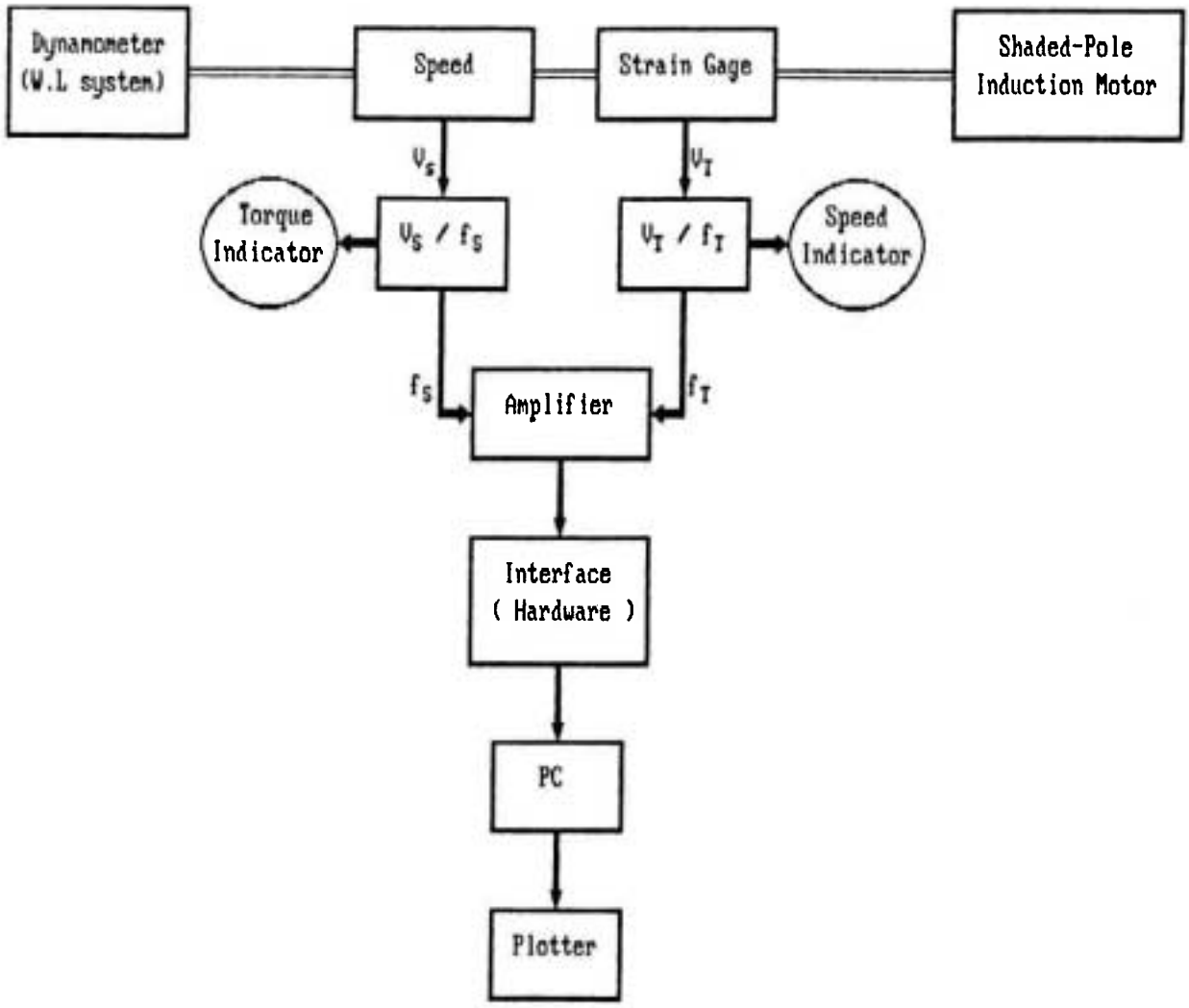

Figure 2. Block diagram of experimental arrangement.

experimental results, when the second method is used. In this range of torque, the motor saturates and thus, the use of the saturated model is preferred. This is the reason for a very large discrepancy between the predicted torque using the first method and the experimental results in the range of T_{st} and T_{po}. For the normal range of operation the first method gives a larger torque compared to measurements. At a speed 400 rpm and the speed corresponding to T_{po}, the first method produces more accurate results than those of the second. As Figure 3 indicates, the torque predicted by the second method, in the range of 100 rpm to 400 rpm, is larger than that of the test values. Slight

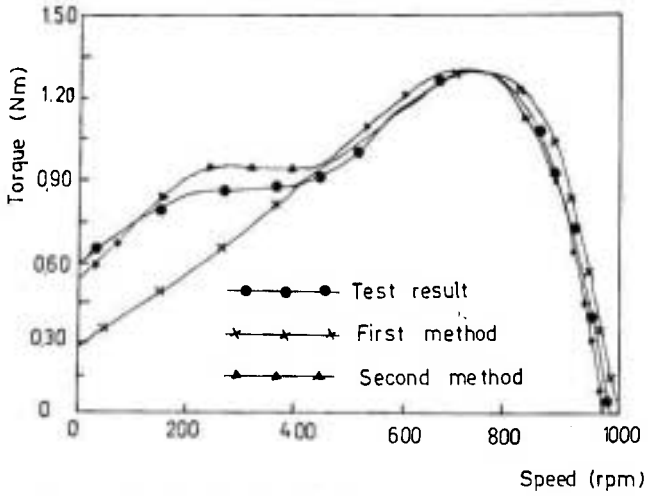

Figure 3. Predicted and measured torque-speed chacteristics.

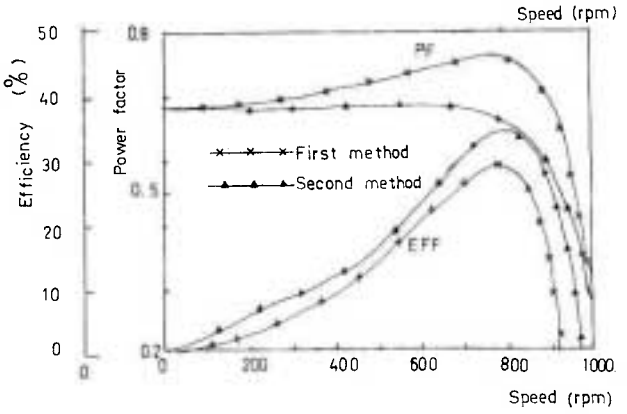

Figure 4. Predicted power factor and efficiency by the first and second methods.

discrepancy between the actual airgap length and the nominal airgap may cause this difference.

Comparison of the power factor versus speed (Figure 4) indicates that except for the speed lower than 200 rpm, in the other ranges, the predicted power factor by the first method is larger than that of the second method; the opposit is true for efficiency. One drawback of the first method is its large predicted power factor; it is not practical to have a power factor as large as 0.78 in a shaded pole induction motor.

Compared to the first method, modelling by the use of the second method offers a more satisfactory result in the whole range of the torque-speed and power factor-speed characteristics.

FLUX DENSITY DISTRIBUTION OVER THE POLE ARC

Flux density due to each harmonic of the main magnetic field is sinusoidal and variation of B crossing the winding will be proportional to the induced *emf*. Suppose the equation of the forward rotating field for harmonic number **n** is as follows:

$$B_{nf} = B_{mnf} \sin(n\theta - wt) \qquad (2)$$

The flux crossing the winding is:

$$\phi = \int_{0\text{-}5(\pi-\theta_m)}^{0\text{-}5(\pi+\theta_m)} B_{mnf} \sin(n\theta - wt)\, l\, r\, (2/P)\, d\theta$$

$$\phi = [(4B_{mnf}.l.r)/(nP)] \sin(n\theta_m/2) \sin(n\pi/2) \cos wt \qquad (3)$$

and induced emf in the main winding resulting from field F is equal to:

$$N_m P\ (d\phi/dt) = [(8B_{mnf} N_m.P.l.r\pi f)/(nP)] \sin(n\theta_m/2) \sin(n\pi/2) \sin wt \qquad (4)$$

To obtain B_{mnf}, the calculated module for each harmonic ($I_m Z_{fn}$) is taken equal to:

$$[(8B_{mnf}N_m.l.r.f.\pi)/n]\sin(n\theta_m/2)\sin(n\pi/2)]$$

Knowing the B_{mnf} due to each harmonic, the equation of the rotating field F can be established. The backward flux density is also as follows:

$$B_{nb} = B_{mnb} \sin(n\theta + wt) \qquad (5)$$

a similar calculation can be performed. Using the same procedure, the induced emf in the q-axis winding can be determined (except that it lags 90 degrees with respect to the reference of the main winding).

Shading angle of d and q shading windings is O_s, but their number of turns is proportional to sinO and cosO. The induced emf of this winding due to field F, $B_{nf} = B_{mnf} \sin(n\theta - wt - \pi/2)$, is now obtained as follows:

$$\phi = \int_{\pi-0.5\theta_s}^{\pi+0.5\theta_s} B_{mnf} \sin(n\theta - wt - \pi/2)\, l.r\, (2/P)\, d\theta$$

$$= 4lrB_{mnf} \sin(n\theta_s/2) \cos wt/(np) \qquad (6)$$

$$\sin(n\theta).P.N_s(d\phi/dt) = \text{Q-axis induced emf}$$
$$= 8B_{mnf}.l.r..f.N_s.\sin(nO)\sin(nO_s/2)].\ (\sin wt)/n \qquad (7)$$

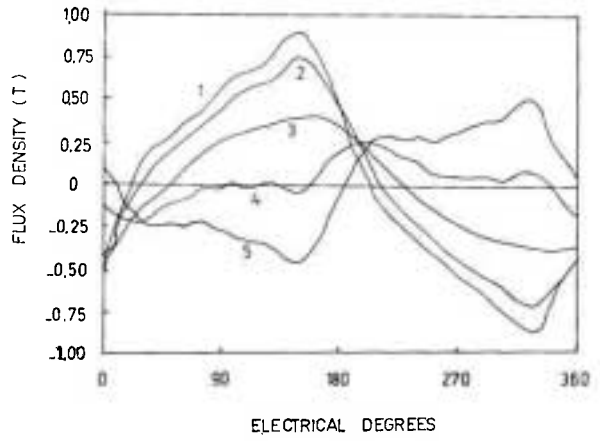

Figure 5. Field distribution in the airgap of the shaded pole for θ_s= 0.497 rad and wt= 0, π/6, π/3, π/2, 2π/3 and 5π/6.

Now in order to obtain B_{mnf}, the calculated module for each harmonic, E_{fsq}, is:

$$E_{fsq} = 8B_{mnf}.l.r\pi f.N_s \sin(n\theta) \sin(n\theta_s/2)]/n \qquad (8)$$

Having B_{mnf} for each harmonic, an equation can be established for rotating F. A similar procedure may be followed for the backward field. These four fields are added up at the same wt and the field waveform over 360 electrical degrees are plotted. Figures 5-7 present the field distribution over the pole for the following conditions: θ_s =

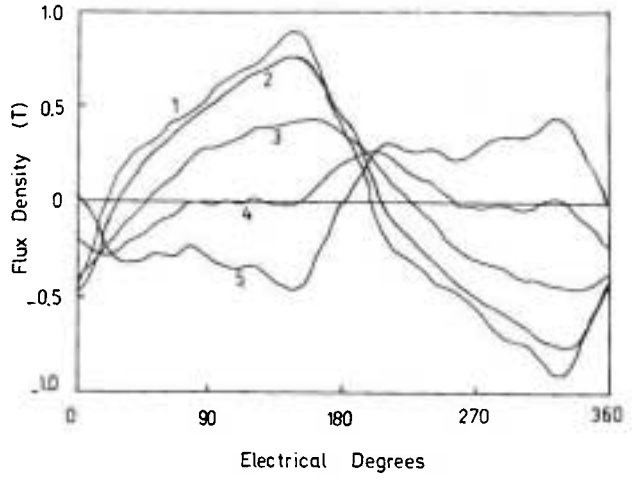

Figure 6. Field distribution in the airgap of the shaded pole for θ_s= 0.597 rad and wt= 0, π/6, π/3, π/2.

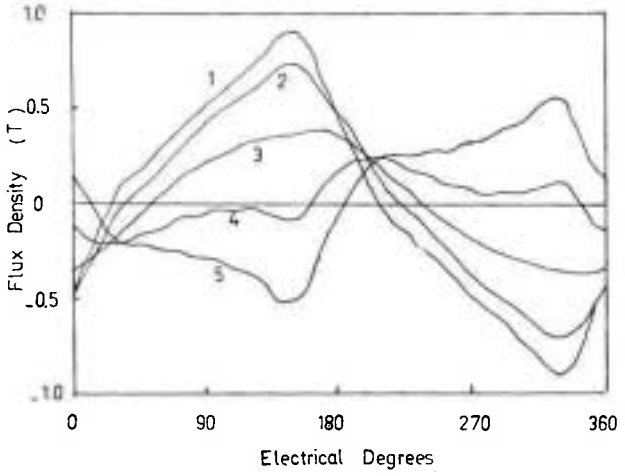

Figure 7. Field distribution in the airgap of the shaded pole for θs= 0.697 rad and wt= 0, π/6, π/3, π/2.

0.497 rad, θ_s = 0.597 rad and θ_s = 0.697 rad, all at wt = 0, π/6, π/3, π/2. and 2π/3, respectively.

The obtained harmonic fluxes show that the fundamental flux does not rotate with a constant speed. Norly its amplitude constant in every cycle (see the curves at instants 1,2,3 and 4 on Figure 8). For instance, between wt = 0 and wt = 30 elec. deg., the rotating magnetic field moves forward by 7 deg., between wt = 30 and wt = 60 deg., it moves forward by 10 deg., and finally between wt = 60 and wt = 90, it moves forward by 72 deg. Such a variation causes a pulsating torque characteristic and generates noise.

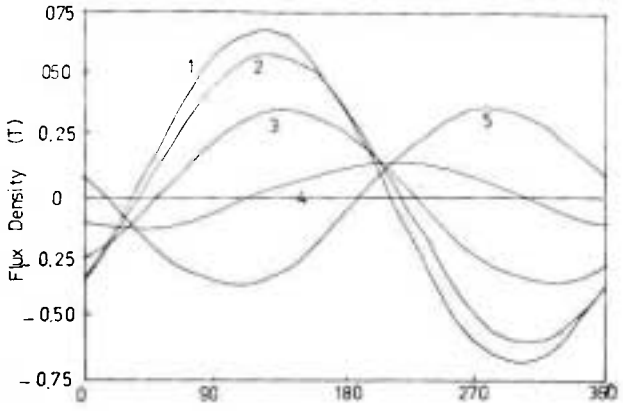

Figure 8. Fundamental flux density wave distribution

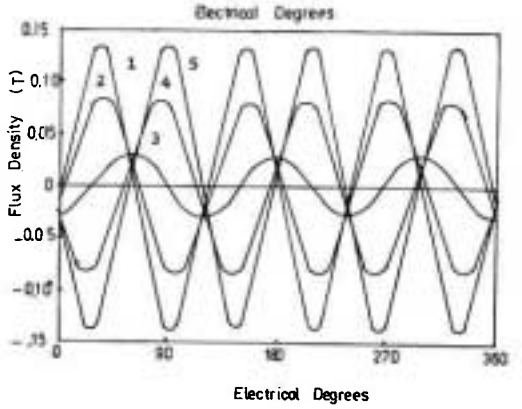

Figure 9. The third harmonic flux density wave distribution.

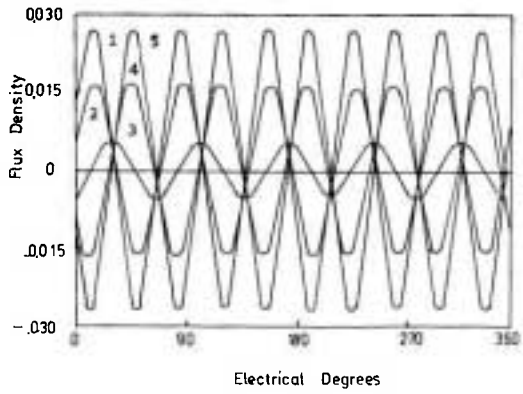

Figure 10. The fifth harmonic flux density wave distribution

The third harmonic (Figure 9) and the fifth harmonic (Figure 10) move forward. For the third harmonic the direction of movement is due to the shading angle and pole angle, since when the "pole arc/ pole pitch" is larger than 0.9 (which is the case in the proposed motor) the developed torque by the third harmonic has the fundamental waveform direction. If this ratio is between 0.6 and 0.9, the third and fundamental flux waveforms will be opposite to each other [13]. The effect of the shading angle upon the flux distribution at wt = 120 is shown in Figure 11.

SATURATION EFFECTS

The effect of saturation upon the motor performance has been ignored in many earlier works [9, 10]. Perret and Pouloujadoff [11, 12] have adopted a step-by-step numerical method to obtain the steady-state characteristics of a saturated shaded pole induction motor. Although Singh [8] has taken into account the saturation using a constant factor (S_{fm}), which is defined as the ratio of the total mmf per pole to the mmf expended in the airgap alone, no justification has been given for such a choice. This constant factor is incoporated in the various reactances estimation.

The design details of the test motor having the following rated values: V=220V, f=50 Hz, P_o=0.125 hp, Pf= 0.6 are given in Table 1.

Motor measured parameters at the rated frequency (referred to the stator) are: R_m= 12.3192 Ω, R_s= 0.00117 Ω and θ_s= 0.597 Elec. rad. The torque-speed characteristic of the test motor is predicted by neglecting saturation, i.e. S_{fm}= 1 (Figure 12). In the linear region of the characteristic, for a fixed torque, the predicted speed is higher than that of the test value. In the remaining part of the torque-speed characteristic, the variation of the predicted torque amplitude is high compared to that of the test torque.

The value of S_{fm} is varied between 1.1 and 1.6 in 0.1 step increments and the performance is predicted for each S_{fm}. The result shows that by increasing the value of S_{fm}, the predicted performance approaches

TABLE 1. Design Details of the Test Motor.

Pole: number = 6, total arc = 56.5 deg., pitch = 34.5 mm
Rotor: diameter = 70.3 mm, bar cross section = 21.204 mm², no. of slots =33, skewing angle = 16.3 deg.
Stator: bore diameter = 71.1 mm, outer diameter = 124 mm, length = 44.45 mm, slot width = 2.7 mm, conductor cross section = 0.195 mm²
Airgap: length = 0.356 mm
Shading: coil span = 5 mm, winding cross section = 1.484 mm², turns/pole = 1, angle = 11 deg.
End ring cross section = 16.129 mm²,
Angle of unshaded part = 45.5 deg.

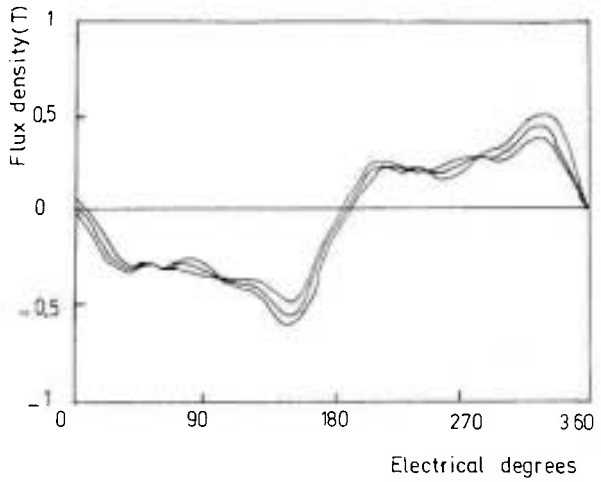

Figure 11. Flux density wave distribution for different shading angle at wt = 120°.

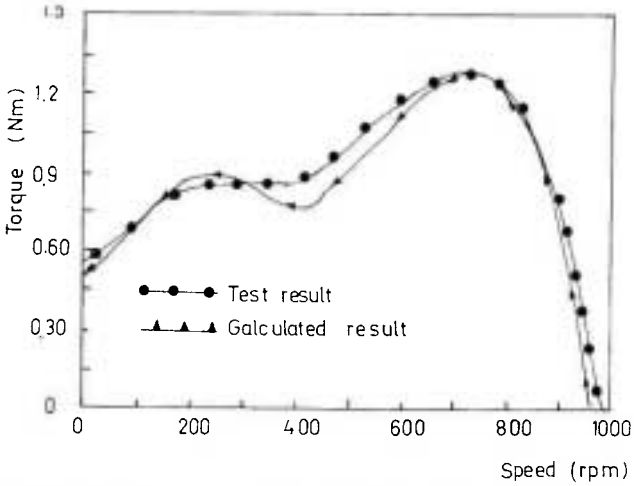

Figure 12. Torque-speed characteristic of the shaded pole induction Motor a: predicted by neglecting saturation b: measured.

the measured performance. By increasing S_{fm} from 1, the torque-speed variations in the starting region gradually reduces and approaches the measured value. On the other hand, pull-out torque of this type of motor increases slightly by increasing S_{fm}.

An increase of S_{fm} from 1.1 to 1.3 gradually improves the predicted values. Increasing S_{fm} to over 1.3, there is less agreement between the predicted and the measured characteristics in the linear region; at this point, the pull-out torque shifts to the lower speed. In contrast with S_{fm}=1, for S_{fm}=1.6 and at a fixed speed, torque in the linear region (the normal operation region) becomes less than that of the measured value.

The Effect of S_{fm} on Starting Torque

Figure 13 indicates that for low and high saturation, the starting toruqe is low with the maximum starting torque occuring for S_{fm} between 1.3 to 1.5. So S_{fm} between 1.3 and 1.5 is taken as convenient values for the saturation factor.

The Effect of S_{fm} on Pull-out Torque

It is deduced from Figure 13 that the rise of the saturation factor from 1 to 1.3 causes an increase of T_{po}. But any increase of S_{fm} over 1.3 does not change T_{po} at all. This reveals that a convenient value of S_{fm} is about 1.3.

The Effect of S_{fm} on Torque at Rated Speed

Figure 13 contains the variation of the torque of the motor at 850 rpm. Considering the torque of 1.02 Nm at the rated speed, there is an agreement between the calculated and test results at S_{fm}= 1.3 for the rated speed.

The Effect of S_{fm} on Rotor Skewing Leakage Reactance

The obtained torque-speed characteristic for rotor skewing leakage reactance which is shown in Figure 14 has a lower starting toque. There is no significant difference between the measured and the predicted values in the linear part of the speed-torque characteristic.

The Effect of S_{fm} on Mutual and Leakage Reactance of the Main Winding

By assuming S_{fm}= 1 in the mutual reactance and the main winding leakage reactance formulea (see Appendix), the torque-speed characteristic has been determined as shown in

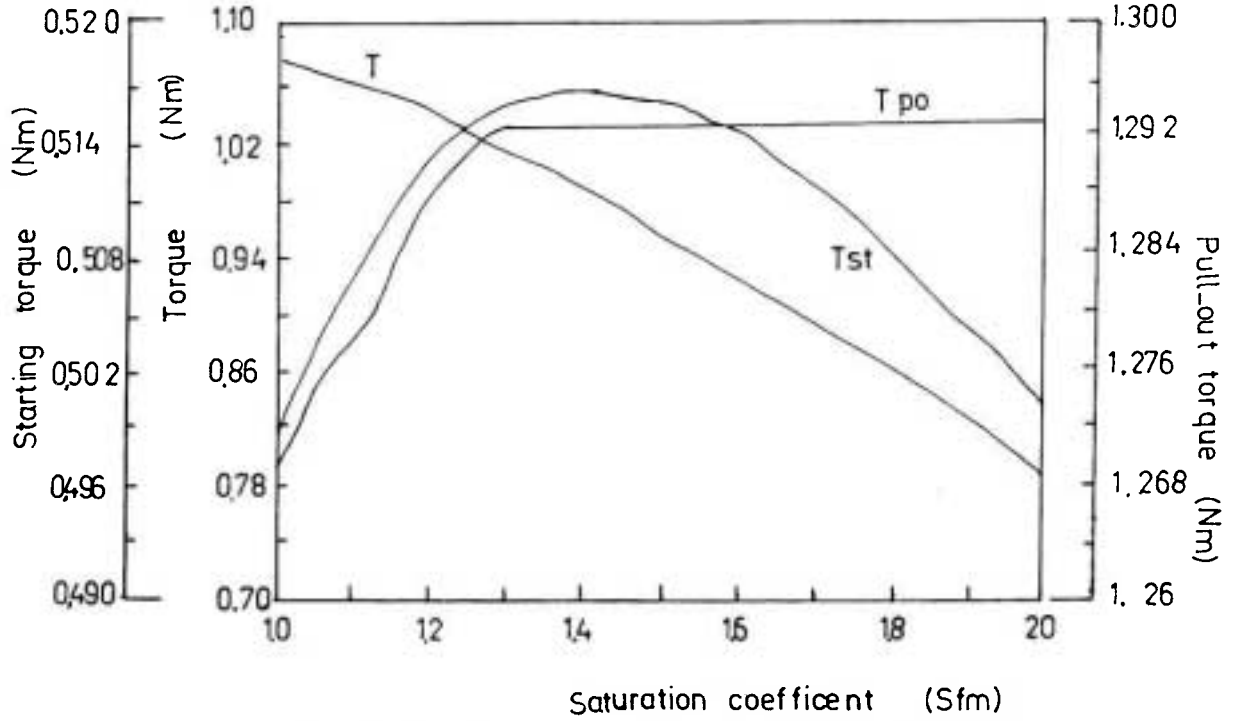

Figure 13. Starting, pull-out and rated torques as a function of S_{fm}.

Figure 15. A comparison with the measured values indicates that there is a rather large difference, particularly between T_{st} and T_{po}. At a fixed torque, the calculated speed is higher than that of the measured speed. In contrast with the previous case (unsaturated rotor skewing leakage reactance), the torque-speed characteristic has changed in the linear portion compared with the experimental characteristic.

These curves prove that the effect of saturation upon the mutual and leakage reactances of the main winding is more significant than on the skewing leakage reactance.

THE EFFECT OF AIRGAP LENGTH

For different values of the airgap length, various characteristics are obtained and presented in

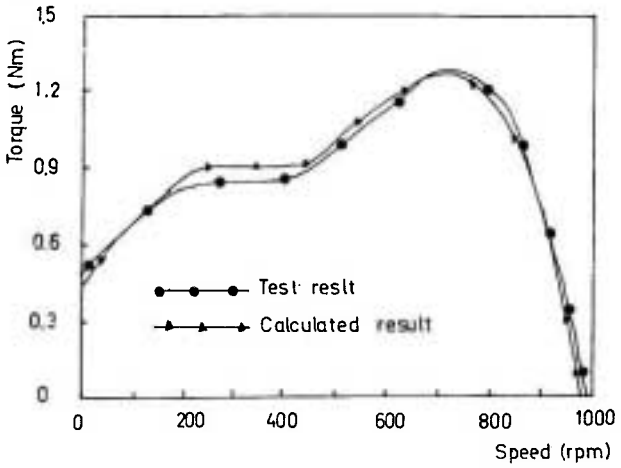

Figure 14. The effect of S_{fm} upon rotor skewing leakage reactance.

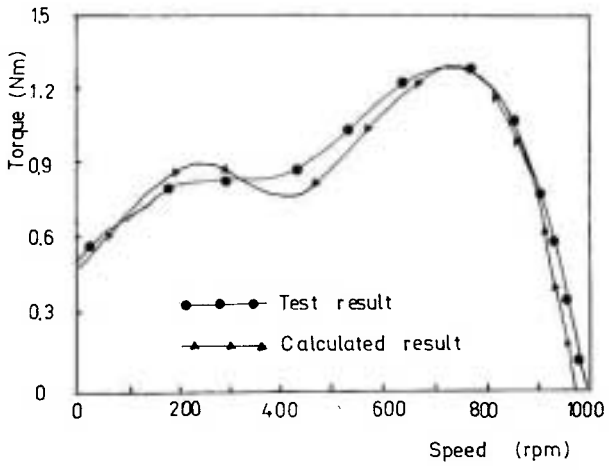

Figure 15. The effect of S_{fm} on mutual and leakage reactance of main winding.

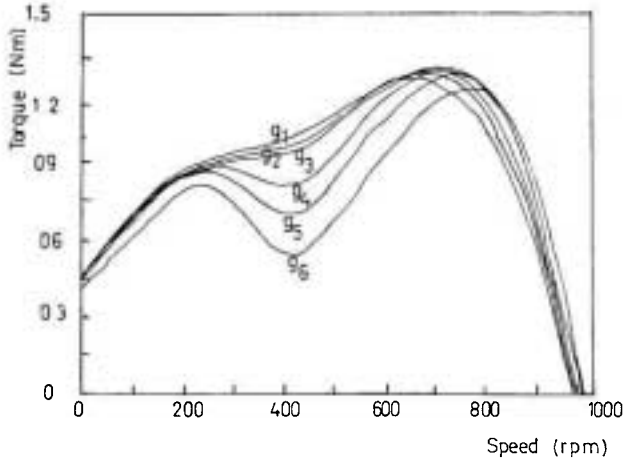

Figure 16. The effect of the airgap length upon torque-speed characteristic

Figure 16. Table 2 shows the variations of the pull-out torque, speed, slip and the hamonic amplitude at wt= 0° for different airgap lengths.

With a decrease of the airgap length, the third harmonic of the flux plays a more significant role in the shaping of the torque-speed characteristic. The iron part of the magnetic circuit of the motor becomes more important when a smaller airgap is proposed. With an increase of the airgap length, the maximum torque occurs at a smaller speed or larger slip. The maximum torque rises up to a particular value of the airgap (0.305 mm) and then drops for any further increase in the airgap.

CONCLUSIONS

Two methods of analysis of shaded-pole induction motors have been used to develop two computer programs for motor performance prediction. Overall, a good agreement was observed between the theoretical results and measurements obtained by using the second method. in which the space harmonics of the airgap flux has been incroporated in the equivalent circuit model of the motor.

For the first time, the equivalent circuits containing harmonic components have been employed in order to predict the flux density distribution over the pole arc of a single phase shaded pole induction motor at different shading angles. The effect of the flux harmonics upon the shape of the torque-speed characteristics was discussed. Saturation was taken into account by incoporating a saturation factor in the various inductance formulea. By comparing the predicted and measured performances, a reasonable range of the saturation factor was suggested.

NOMENCLATURE

f	Frequency	Hz

TABLE 2. Airgap Effect.

Airgap length (mm)	**g_1 0.508**	**g_2 0.457**	**g_3 0.406**	**g_4 0.305**	**g_5 0.254**	**g_6 0.203**
T_{max} (Nm)	1.254	1.277	1.292	1.293	1.265	1.205
Speed (rpm)	660	680	710	730	750	760
s	0.340	0.320	0.290	0.270	0.250	0.240
Amp. of lst har.	0.259	0.250	0.240	0.221	0.219	0.228
Amp. of 3rd har.	0.125	0.133	0.142	0.164	0.176	0.184
Amp. of 5th har.	0.0412	0.0484	0.0516	0.0623	0.0714	0.085
Amp. of 7th har.	0.0250	0.0251	0.0218	0.0310	0.0325	0.032
Amp. of 9th har.	0.0120	0.0132	0.0155	0.0228	0.0268	0.032

Note: Amp. = Amplitude, har. = harmonic

l	Stator stack length	m
r	Mean radius of rotor	m
T_{st}	Starting torque	Nm
T_{po}	Pull out torque	Nm
i_m	Main winding current	A
Z_{fn}	Forward impedance for harmonic number n	Ω
Z_{bn}	Backward impedance for harmonic number n	Ω
X_l	Leakage reactance of stator main winding	Ω
X_m	Mutual reactance	Ω
B_{nf}	Forward flux density for harmonic number n	T
B_{mnf}	Max. forward flux density for harmonic number n	T
B_{nb}	Backward flux density for harmonic number n	T
B_{mnb}	Max. backward flux density for harmonic number n	T
w	Angular velocity	rad/sec
θ_s	Shading angle (Electrical)	rad
θ_m	Main pole angle (Electrical)	rad
θ	$(\theta_m-\theta_s)/2$	rad
E	Emf	V
P	Number of pole	
n	Harmonic number index	
m	Index for main winding	
s	Index for shading coils	
f	Index for forward wave	
b	Index for backward wave	
S_{fm}	Saturation factor	
N	Number of turns	
r_{fs}, r_{fm}	Core loss equivalent resistances	Ω
K_{wsn}	Winding factor of shading coils for harmonic no. n	
K_{wmn}	Winding factor of main winding for harmonic no. n	
E_n	Induced speed emf resulting from rotating fields	V

REFERENCES

1. P. H. Trickey, "An Analysis of the Shaded Pole Motor", *AIEE Trans.*, Vol. 55, (1936), 1007-1014.
2. P. H. Trickey, "Performance Calculation on Shaded-pole Motor", *AIEE Trans.*, Vol. 66, (1947), 1431-1438.
3. S. S. L. Chang, "Equivalent Circuit and Their Applications in Designing Shaded Pole Motors", *AIEE, Tran.*, 70, (1951), 690-699.
4. H. Ooka, "Analysis of the Reluctance Augmented Shaded Pole Motor", *IEE. J.*, 91 (1971), 2117-2125.
5. H. Ooka "Effect of Parameter Changes on the Torque of Shaded Pole Motors", *IEE. J.*, 92B, (1972), 78-87.
6. O. L. Butler and A. K. Wallace," Effect of Parameter Changes on the Performance of Shaded Pole Motors", *Proc. IEE.*, 116, No. 5, (1969), 732-736.
7. T. Yokozuka, "Alternating Torque Characteristics of the Shaded Pole Motor", *IEE. J.*, 99B, (1979), 737-747.
8. B. Singh, "Revolving Field Analysis of a Shaded Pole Motor", *IEEE Trans.*, Vol. PAS-102, No. 4, (April 1983).
9. R. Perrer and M. Poloujadoff, "Characteristics Analysis of Saturated Pole Motor", *IEEE Trans.*, Vol. PAS-90, No. 2, (1971), 484-494.
10. M. Poloujadoff, "General Rotating mmf Theory of Squirrel Cage Induction Machines with Non-uniform Airgap and Several Non-sinusoidally Distributed Windings", *IEEE Trans.*, Vol. PAS-101, No. 3, (1982), 583-591.
11. B. G. Desai and M. A. Mathew", Transient Analysis of Shaded Pole Motors", *IEEE Trans.*, Vol. PAS-90, No. 2, (1982), 484-494.
12. K. Makowshi and K. Schoepp, "An Analysis of Shaded Pole Induction Motors with Increased Starting Torque," *Elec. Machines and Power Systems*, Vol. 8, (1983), 419-432.
13. A. G. Say, "Alternating Current Machines", Fifth Edition, Pitman (1987).

APPENDIX A

Main Winding Mutual Reactance

$$X_{mn}=2.\pi.f.N_m^2K_{wmn}^2.C_{skn}.10^{-8}\ (0.647L_2.\lambda_{2\lambda pn})/g_e\ .n.P.S_{fm}\lambda_{pn} \quad (A.1)$$

where λ_{pn} = pole pitch for harmonic number n (in)

$= \pi\ (D_2+g_e)\ /\ (nP)$

D_2= rotor outer diameter (in.), g_e= airgap effective length

$C_{skn} = \sin(n\theta_{sk}/2) / (0.5\, n\theta_{sk})$

Main Winding Leakage Reactance

$$X_l = 2\pi f.N_m^2.K_{wml}^2.10^{-8}\,[(3.19L_1.K_{sl} + L_{el}) / 2P + (3.19L_2\lambda_{pl}.\theta_m) / (4g_e.P.\pi.S_{fm})] - \sum_n X_{mn} \quad (A.2)$$

where L_1= stator axial length, K_{sl}= slot constant of winding L_{el}= main winding cover (in.), λ_{pl}= pole pitch for fundamental field (in.).